Ketogenic diet-mediated steroid metabolism reprogramming improves the immune microenvironment and myelin growth in spinal cord injury rats according to gene and co-expression network analyses

Hong Zeng[1,2,*], Yao Lu[1,*], Meng-Jie Huang[1], Yan-Yan Yang[1], Hua-Yi Xing[1], Xiao-Xie Liu[1], Mou-Wang Zhou[1]

[1]Department of Rehabilitation Medicine, Peking University Third Hospital, Beijing 100191, China
[2]Department of Rehabilitation Medicine, Shanghai Ninth People's Hospital Affiliated to Shanghai Jiao Tong University School of Medicine, Huangpu 200011, China
*Equal contribution

Correspondence to: Mou-Wang Zhou; email: zhoumouwang@163.com, https://orcid.org/0000-0003-1553-0613
Keywords: spinal cord injury, ketogenic diet, RNA-seq, steroid biosynthesis, metabolic reprogramming, immune microenvironment
Received: October 23, 2020　　Accepted: March 27, 2021　　Published: May 6, 2021

ABSTRACT

The ketogenic diet has been widely used in the treatment of various nervous system and metabolic-related diseases. Our previous research found that a ketogenic diet exerts a protective effect and promotes functional recovery after spinal cord injury. However, the mechanism of action is still unclear. In this study, different dietary feeding methods were used, and myelin expression and gene level changes were detected among different groups. We established 15 RNA-seq cDNA libraries from among 4 different groups. First, KEGG pathway enrichment of upregulated differentially expressed genes and gene set enrichment analysis of the ketogenic diet and normal diet groups indicated that a ketogenic diet significantly improved the steroid anabolic pathway in rats with spinal cord injury. Through cluster analysis, protein-protein interaction analysis and visualization of iPath metabolic pathways, it was determined that Sqle, Sc5d, Cyp51, Dhcr24, Msmo1, Hsd17b7, and Fdft1 expression changed significantly. Second, through weighted gene co-expression network analysis showed that rats fed a ketogenic diet showed a significant reduction in the expression of genes involved in immune-related pathways, including those associated with immunity and infectious diseases. A ketogenic diet may improve the immune microenvironment and myelin growth in rats with spinal cord injury through reprogramming of steroid metabolism.

INTRODUCTION

Spinal cord injury (SCI) is a devastating event that can lead to neurological deficits and motor dysfunction [1–2]. The dysfunction of motor and sensory functions after SCI is caused by two processes: primary injury and secondary injury. Primary injury results from irreversible mechanical damage to the spinal cord, which directly damages various tissue components. In contrast, secondary injury is a cascade of effects triggered by primary injury that

presents as a variety of biochemical and pathological events, such as oedema, inflammation and apoptosis [3–4]. Current treatment strategies for SCI aim to protect neurons from secondary damage [5–6]. However, therapy is effective only in a limited scope [7]. Thus, understanding the molecular changes in SCI after therapy could lead to improved treatment of patients with SCI.

A ketogenic diet (KD) is a high-fat, low-carbohydrate, moderate-protein diet that results in the prominent

production of ketone bodies (KBs: β-hydroxybutyrate [BHB], acetoacetate [ACA] and acetone) [8]. Furthermore, the KD has been validated as an effective non-pharmacological preventive treatment for drug-resistant epilepsy [9–10]. Interestingly, recent studies have suggested that a KD might also be beneficial to humans with neurological disorders, such as Parkinson's disease, Alzheimer's disease, multiple sclerosis, and traumatic brain injury [11–13]. Multiple reports have revealed that a KD may exert neuroprotective effects after SCI [14–19]. For example, Tetzlaff et al. found that KD improves forelimb motor function after SCI [14]. Zhu et al. revealed that a KD exerts neuroprotective effects by attenuating oxidative stress in SCI rats [18–19]. Finally, our study recently reported that a KD improves motor function by activating Nrf2 and suppressing the NF-κB signalling pathway to attenuate oxidative stress and inflammation after SCI [17]. However, the underlying mechanisms by which a KD provides neuroprotection after SCI are still not fully understood.

Based on the above information, in this study, we performed RNA sequencing (RNA-seq) to examine the changes in the gene expression of spinal cord tissue in Sprague-Dawley rats under with different conditions. We identified differentially expressed genes (DEGs) and comprehensively detected genes with important biological significance through gene set enrichment analysis (GSEA) at the overall level [20]. Weighted gene co-expression network analysis (WGCNA) was used to establish a gene co-expression network to explore the relationship between the gene network and the KD diet phenotype [21]. These data promote further understanding of the new genes and related signalling pathways and how KD treatment improves the recovery of motor function in SCI rats, providing new guidance for clinical treatment.

RESULTS

Experimental procedures and animal conditions

The entire experimental process is shown in Figure 1A. To establish a C7 spinal cord hemi-contusion model, unilateral C7 laminectomies were performed using a Precision Systems and Instrumentation-IH Impactor according to the manufacturer's instructions (Supplementary Figure 1A). Sprague-Dawley rats were anaesthetized with sodium pentobarbital to expose the spinal cord. We fixed the C6-T1 vertebrae rigidly in a frame tilted at a 25.0° angle and then used the Infinite Horizon impactor to deliver a set contusion force of 150 kdyne (Supplementary Figure 1B); the contusion forces were monitored by a computer (Supplementary Figure 1C). An average of 150 kdyne contusion force was obtained for each sample. These results indicated that

the C7 spinal cord hemi-contusion model was successful. Based on myelin staining, the myelin sheath area in the SCI_KD group was significantly larger than that in the spinal cord injury with standard diet (SCI_SD) group (Figure 1B–1C), indicating that SCI rats exhibited protection or promotion of myelin sheath growth at the injured site after feeding with a KD.

Differentially expressed mRNAs

To further understand the effects and mechanism of the KD on SCI, RNA-seq was performed on each group with 5 biological replicate samples, in which 5 samples were degraded and eliminated. To explore transcription factor expression in Sprague-Dawley rats treated with the KD under spinal cord injury, we established 15 RNA-seq cDNA libraries from the rats divided into 4 groups (SCI_KD, SCI_SD, Sham_KD, and Sham_SD). A summary of the sequence assembly after Illumina sequencing is presented in Supplementary Table 1. The average of raw reads was 23295214.7, the Q30 basic mass fraction of the sample was 100%, and the error rate (%) was 0, meeting the requirements for subsequent analysis. Using a comparison of the transcriptome and reference genome, greater than 82% of reads were uniquely mapped; these results met the subsequent analysis requirements (Supplementary Table 2). In short, the sequencing data were suitable for subsequent data analysis.

A total of 32,883 genes were detected by RNA-seq, and Venn analysis between samples showed the number of expressed genes in each group (Figure 2A). We first used an unsupervised classification method-principal component analysis (PCA) to characterize the differences among the gene expression profiles of the 15 samples. Figure 2C shows that the biologically replicated samples could be divided into the following 4 groups: Sham_SD1-3, Sham_KD1-4, SCI_SD1-3 and SCI_KD1-5. A PCA model showed that the maximum variation in PC1 could explain 16.92% of the variation, while principal component 2 explained 9.85% of the variation [11]. In Figure 2B, the scatter plot of differential genes between the SCI_KD and SCI_SD groups shows that 463 genes were differentially expressed between the two groups, among which 184 DEGs were upregulated, and 279 DEGs were down-regulated. The top 50 upregulated and downregulated genes are listed in Supplementary Tables 3 and 4, respectively.

Reprogramming steroid biosynthesis and metabolism in SCI rats on KD

Compared with the SCI_SD group, the KD group exhibited upregulated DEGs in many enrichment

pathways, such as the steroid synthesis pathway in lipid metabolism (path ID: map00100, q-value = 5.82043E-08), biosynthesis of unsaturated fatty acids, terpenoid backbone biosynthesis, etc. A bubble chart of the DEGs in the top 20 most enriched pathways is provided (Figure 3A). The downregulated DEGs from the KD diet group were significantly enriched in ribosomes, lysosomes, osteoclast differentiation, proteasome, tuberculosis, and antigen processing and display. Figure 3B shows the KEGG enrichment distribution of the DEGs.

To further understand the biological functions of the SCI_SD and SCI_KD DEGs, we performed gene set enrichment analysis (GSEA) of the sample sets based on the C2 MSigDB database, which includes the Broad Institute recombined gene sets. The selected gene set was tested, and it was found that SCI_KD was significantly negatively correlated with inflammatory cytokines and their receptors (the NES values were –1.44 and –1.46, respectively; Supplementary Figure 2), suggesting that a KD reduces the lethality of SCI, which echoes the results of our previous studies. Similarly, based on the KEGG functional annotation, we found that SCI_KD was significantly positively correlated with the steroid synthesis pathway (the NES is 1.62; Figure 3C) by GSEA analysis, which further shows that the KD is involved in the metabolic reprogramming of steroids in SCI rats, which is a positive effect of the KD. An important mechanism of SCI function may be related to reducing metabolic responses. iPath3.0 was used to visually analyse the enriched steroid metabolism-related genes, as shown in Supplementary Figure 3, which shows that the steroid metabolism DEGs in the biological system transmit information.
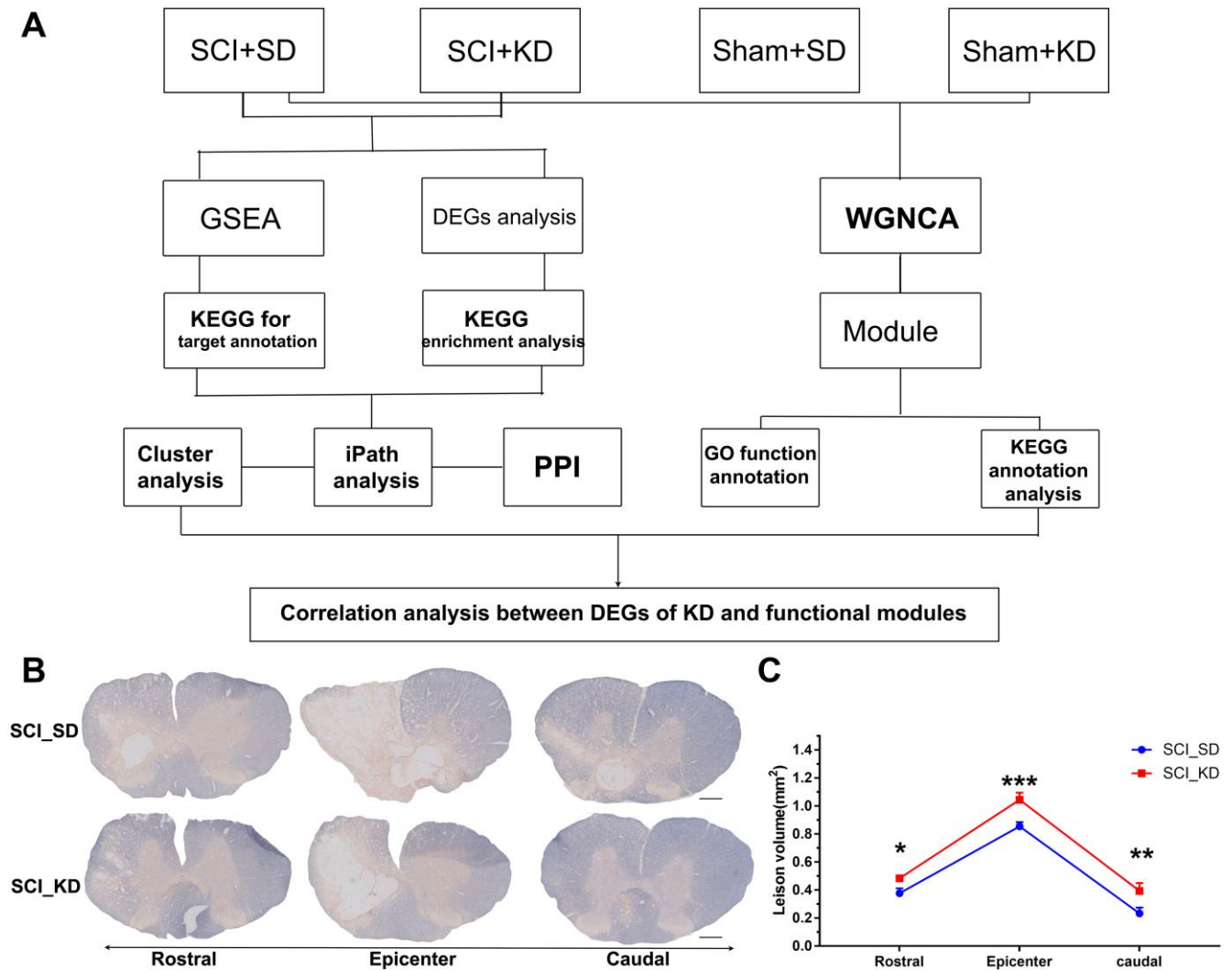

Figure 1. Experimental protocol and animal myelin area. (**A**) Detailed experimental protocol. (**B**) Representative images showing EC staining after SCI. Scale bar = 1 mm. (**C**) Quantitative analysis of the results in panel (A). All data are presented as the mean ± standard deviation, n = 3. Rostral of the injury site, p = 0.0255; Epicentre, p = 0.0004; Caudal, p = 0.0015.

Cluster analysis and PPI analysis of DEGs in the steroid synthesis pathway

Figure 3D shows that the *Sqle* (squalene epoxidase), *Sc5d* (sterol-C5-desaturase), *Cyp51* (cytochrome P450, family 51), *Dhcr24* (24-dehydrocholesterol reductase), *Msmo1* (methylsterol monooxygenase 1), *Hsd17b7* (hydroxysteroid (17-β) dehydrogenase 7), and *Fdft1* (farnesyl diphosphate farnesyltransferase 1) genes were obviously highly expressed in the SCI_KD group. DEGs corresponded to interaction relationships for network

integration and allowed us to identify key pathways in the interaction network according to indicators such as the connectivity between genes (Figure 3E).

WGCNA and hub module identification and analysis

According to the KEGG enrichment analysis of differential gene expression and the GSEA, the mean values showed that SCI rats in the KD group exhibited significantly increased steroid anabolism, which
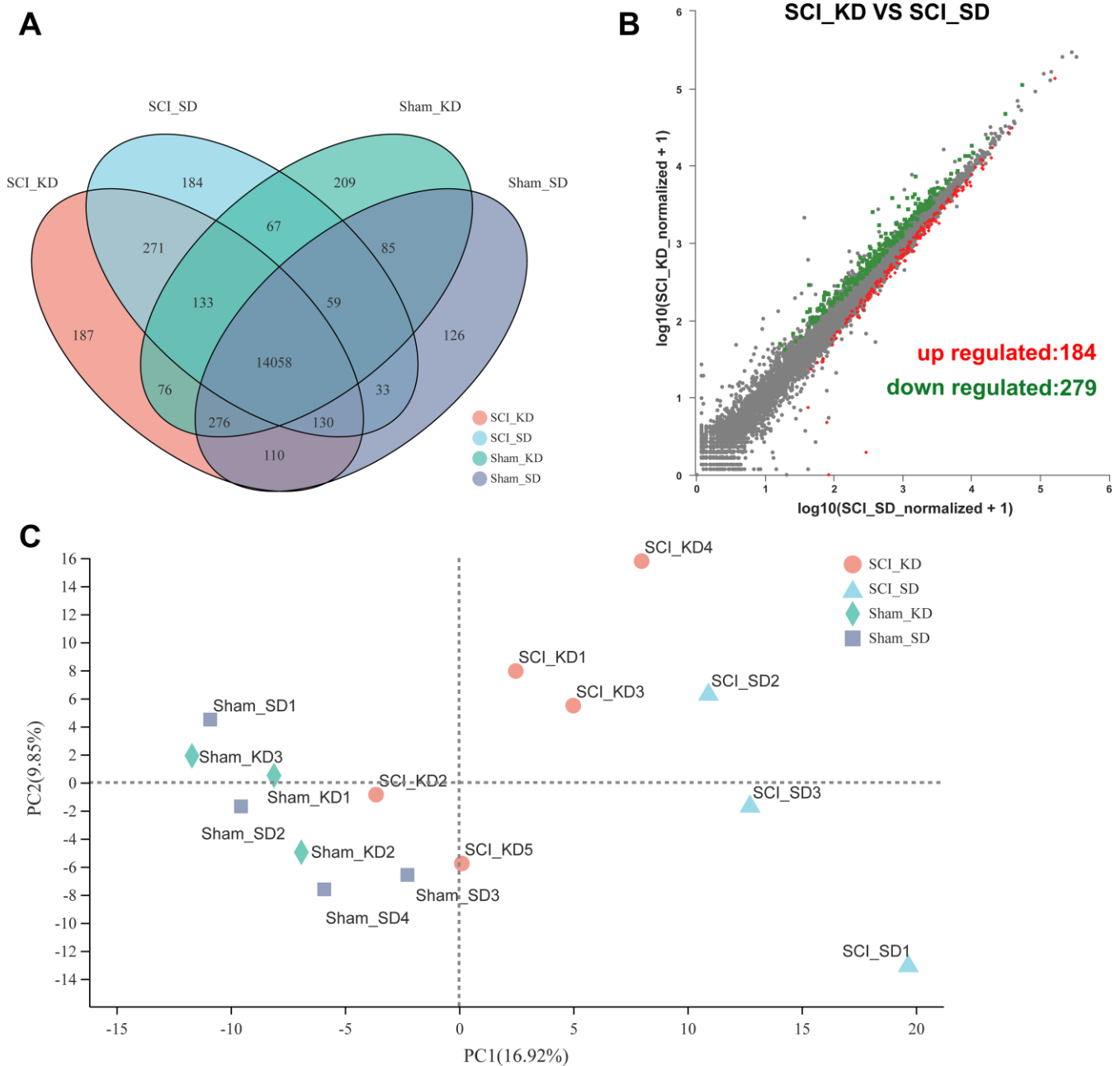

Figure 2. Changes in mRNA expression profiles between groups. (**A**) The mRNA expression of the four groups in the entire transcriptome. (**B**) Volcano plots showing the up- and downregulated mRNA transcripts in the SCI_KD vs. the SCI_SD group. (**C**) Principal component analysis (PCA) score plot with the two principal components (PC1 = 16.92%; PC2 = 9.85%).

indicates that the KD may be protective by mediating steroid metabolism reprogramming. By changing certain physiological functions or pathways, we could analyse the SCI_KD, SCI_SD, Sham_KD, and Sham_SD results in a gene network (WGCNA) and fully understand the roles of a KD and standard diet (SD) on genetic changes in Sprague-Dawley rats. Genes that were commonly expressed in the four groups were placed in the same gene network through the WGCNA algorithm. A total of 32,883 mRNAs were screened by WGCNA, and a total of 5,163 mRNAs were used for subsequent analysis after pre-processing and filtering, such as excluding deletions and outliers. Figure 4A and 4B show the scale-free fitness curve and the average connectivity curve, respectively. The scale-free fitness

curve is in a smooth position, and the power exponent is a weighted β value; thus, the soft threshold value is set to 6, and the scale-free topological index is 0.9. Therefore, the network conforms to the power law distribution and is close to the actual biological network state. The resulting gene tree diagram and the colours in the corresponding modules are shown in Supplementary Figure 4A–4B, with the number of mRNAs for each module shown in Supplementary Table 5.

After the data were pre-processed, the genes were classified, and genes with similar expression patterns were divided into categories called modules. We performed module clustering and module correlation analysis for the obtained modules, as shown in Figure 4D. Interaction
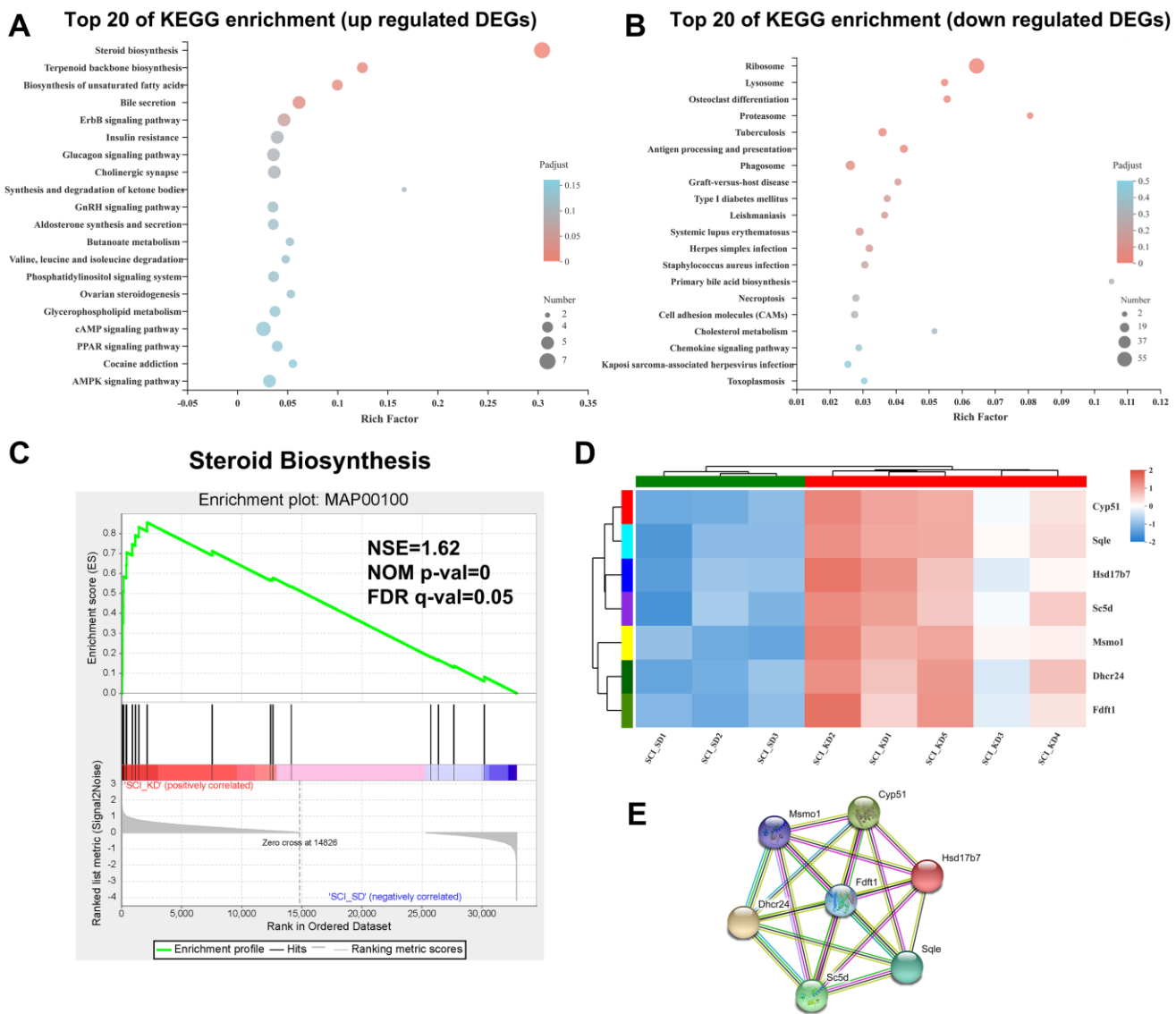

Figure 3. Enrichment analysis of DEGs in the SCI_KD vs. the SCI_SD group. (**A**) KEGG enrichment bubble diagram of the upregulated DEGs from the SCI_KD and SCI_SD groups. (**B**) KEGG enrichment bubble diagram of the downregulated DEGs from the SCI_KD and SCI_SD groups. (**C**) The GSEA analysis diagram of steroid biosynthesis between SCI_KD and SCI_SD. (**D**) Cluster analysis of KEGG-enriched DEGs. (**E**) Protein-protein interaction of DEGs between the SCI_KD and SCI_SD groups.

relationships were analysed in the six different modules, and a network heat map of the correlation between the modules and the phenotype was drawn (Figure 4C). The results show that the modules are independent of one another, which indicates the relative independence of gene expression in different modules. Here, we mainly analysed the correlation modules between the KD- and SD-fed rats. Among them, the MEgreen module is highly related to a KD, and the MEblue module is highly related to a SD. We then calculated the correlation coefficient between each gene in the module and specific phenotype data to obtain the gene significance (GS) value; this value was combined with the MM value of each gene in the module (i.e., kME, eigengene-based connectivity) to obtain the MM-GS scatter plot. The stronger the correlation, the closer the relationship between the module and the phenotype; moreover, correlations with a lower p-value are more reliable. This analysis shows that MEgreen is an important module in the KD, while MEblue is an important module in the SD (Supplementary Figure 4C–4F).
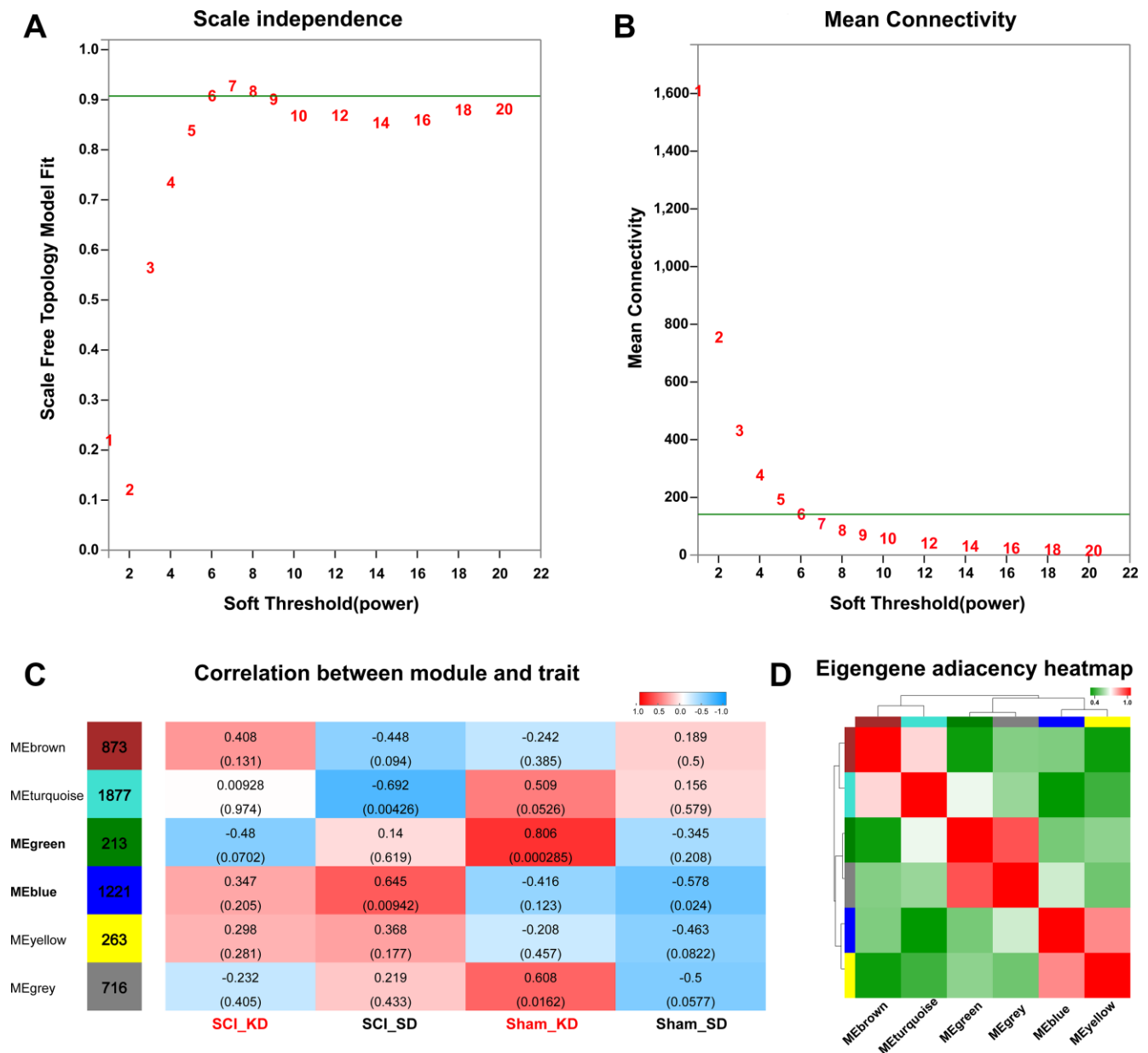

Figure 4. Data pre-processing and module identification for WGCNA analysis. (**A–B**) Analysis of the network topology with different soft threshold powers. The left panel shows the influence of soft threshold power on the scale-free topology fitting index. The right panel shows the influence of soft threshold power on the average connectivity. (**C**) Analysis of the correlation between the module and the diet phenotype. Red indicates that the module has a higher correlation with the phenotype, while blue means the module has a lower correlation with the phenotype. (**D**) WGCNA module correlation; the colour indicates the correlation between modules.

Functional annotation analysis of hub modular genes

To explore the biological functions of the KD and SD modules (green and blue, respectively) and compare the differences in their biological functions, we performed GO and KEGG enrichment analysis with annotation and visualization. GO function annotation analysis classifies DEGs using different perspectives, such as the biological processes involved, the components that constitute cells, and the molecular functions achieved. Figure 5A shows the GO annotation functions of the MEgreen module, and Figure 5B shows the GO annotation functions of the MEblue module. Different from other groups, there was a significant positive correlation between SCI rats that received a SD and the MEblue module. GO functional analysis of immune system processes is expressed as biological processes, which indicated that the immune system significantly affected SCI rats, and immune system processes included all processes of inflammation-related pathways and congenital and acquired immune expression changes.

Similarly, KEGG annotation analysis was also performed on the green and blue modules. The results showed that the KEGG annotation molecule in the MEblue module significantly identified immune system, immune system and infectious diseases: viruses and other immune disease pathways among the subtypes. This module mainly focused on rats with SCI that received a SD, which is consistent with the GO function analysis results. Compared with the MEblue module, in terms of expression ratio, immune system, immune system and infectious diseases with the sub-categories of viruses and other immune disease pathways were significantly downregulated, and the module is related to the KD (Supplementary Figure 5).

Multi-gene set KEGG enrichment analysis and gene interaction network analysis

The immune system and infectious diseases: viral and immune disease pathways were used as pathways of interest for multi-gene KEGG enrichment analysis. Figure 6A shows the KEGG enrichment results of the MEgreen module, and Figure 6B shows the KEGG enrichment results of the MEblue module. The MEgreen module is primarily a module closely related to the KD rats, while the MEblue module is mainly a module closely linked to the SD rats, especially the SD injury rats. The results of the KEGG enrichment signal pathways and intersection of the top 20 pathways for the two modules show that only the viral myocarditis and phagosome pathways are present in both modules. The MEgreen module mainly activates innate immune-related pathways, such as the Toll-like receptor signalling pathway and the NOD-like receptor signalling pathway. These results indicate that MEgreen and MEblue act on different immune pathways. The WGCNA and functional analysis showed that rats fed a KD showed a reduction in immune system pathway processes, including immune diseases, infectious diseases and other immune microenvironments.
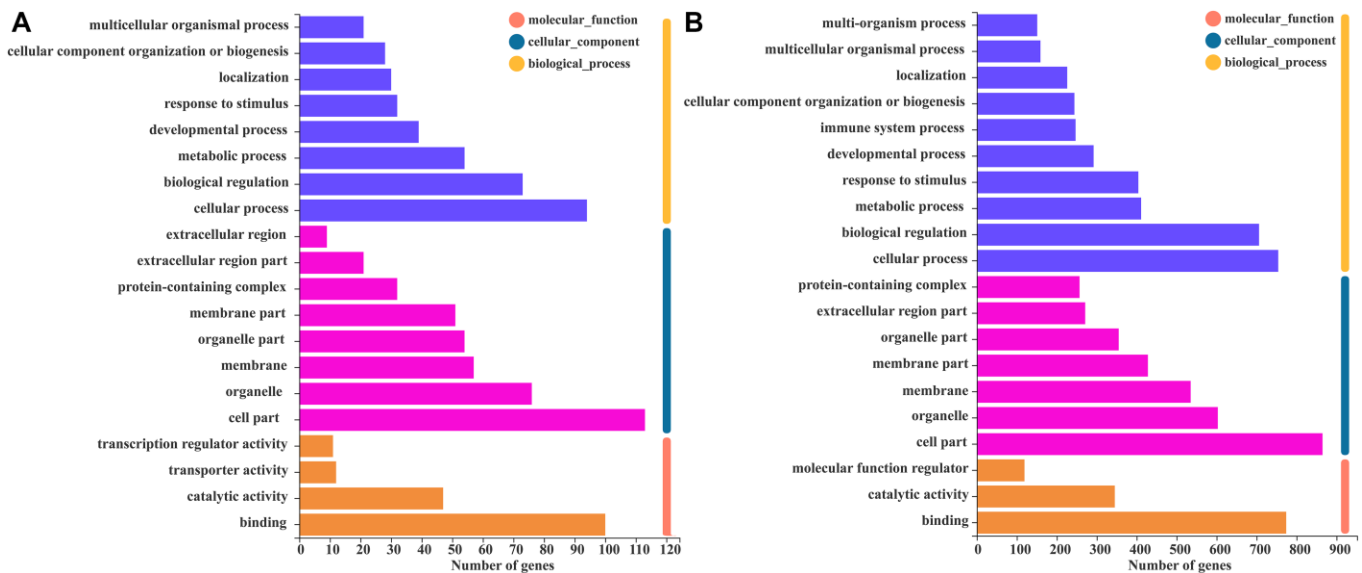

Figure 5. GO function annotation analysis of WGCNA module genes. (**A**) The GO function annotation analysis histogram of the MEgreen module. (**B**) The GO function annotation analysis histogram of the MEblue module, which includes biological processes, cell components, and molecular functions.

DISCUSSION

The KD has been widely used in the treatment of a variety of neurological and metabolism-related diseases, especially epilepsy [22–23]. In recent years, some studies, including previous studies performed by our team, have shown that the KD has a protective effect after SCI by increasing spontaneous movement and fine manipulation in SCI animal models [17, 24–25]. However, the mechanism of action of the treatment is
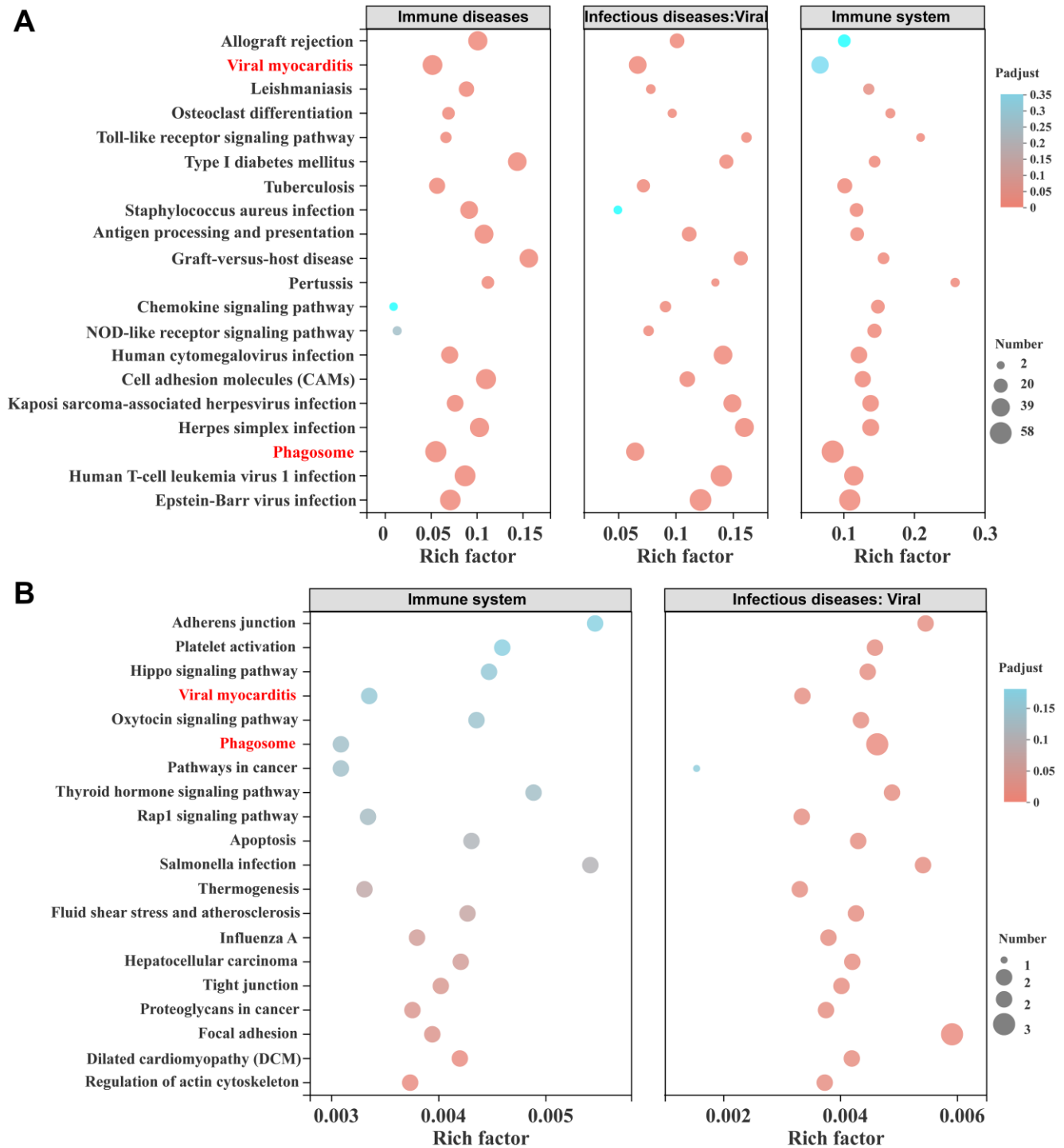

Figure 6. Multi-gene set KEGG enrichment analysis and modular gene visualization. (**A**) The bubble diagram of the intersection of the KEGG pathway in the MEblue module, including the immune system and infectious diseases: viral and immune diseases gene sets. (**B**) The bubble diagram of the intersection of the KEGG pathway in the MEgreen module, including the immune system and infectious diseases: viral gene sets.

still unclear. In this study, myelin expression and transcriptome level changes between different groups were detected in rats under different dietary feeding methods. This study is the first to use RNA-seq to understand and identify DEGs in SCI rats fed a KD and then examine which biological signalling pathways can explain the protective effects of the KD diet on SCI rats.

We used a variety of analytical methods to mine and interpret entire transcriptome RNA-seq data, including DEG and functional enrichment analysis between groups, GSEA between groups, iPath metabolic pathway analysis, gene cluster analysis, WGCNA and module analysis, module function analysis and gene interaction network analysis. From single-gene expression analysis to changes in the overall gene network, a comprehensive analysis of the changes in gene expression patterns under a KD can provide a deeper understanding of the changes in gene transcription and signal pathways induced by a KD for the treatment of SCI.

From a local perspective, we used KEGG pathway enrichment of upregulated DEGs in the SCI_KD and SCI_SD groups and GSEA analysis of these groups to reach a consistent conclusion that KD significantly increased the steroid anabolic pathway in rats with SCI. Through cluster analysis, PPI analysis and the iPath metabolic pathway visualization, we concluded that *Sqle, Sc5d, Cyp51, Dhcr24, Msmo1, Hsd17b7,* and *Fdft1* expression changed significantly in the pathway. Steroid biosynthesis appears to play a pivotal role in SCI.

The KD is a high-fat, low-carbohydrate and moderate-protein diet. Its purpose is to reduce carbohydrate intake and replace it with lipids, while ensuring a sufficient protein supply [26]. This programme was proposed by Wilder in 1921 for the treatment of epilepsy. It was later used for a variety of neurological diseases, such as Alzheimer's disease, Parkinson's disease, etc. [9, 27]. Although it is known that a KD promotes high ketone body levels, high fat, low carbohydrates, low calories and other "immediacy" properties [28–29], this study suggests that the KD may mediate steroid metabolism reprogramming to treat SCI in rats. As an alternative method to transiently raise systemic ketone body levels, most individuals practice the KD, this dietary approach can (1) decrease hepatic de novo lipogenesis; (2) alleviate low-grade chronic inflammation; (3) abate hyperglycemia; (4) elevate systemic β-hydroxybutryate levels, which reflects an increase in β-oxidation; and (5) promote the abundance of folate-producing Streptococcus in the gut, which further up-regulates folate-dependent one-carbon (-CH3) metabolism [30].

This study is the first to reach this conclusion. Steroids include sterols (such as cholesterol, lanosterol, sitosterol, stigmasterol, and ergosterol), bile acids and bile alcohols, steroid hormones (such as adrenal cortex hormones, androgens, and oestrogen), insect ecdysone, cardiac glycosides, saponins, and toad poison [31–33]. Eating a high-fat/low-carbohydrate KD can cause the liver to produce ketones. In the brain, ketone bodies (such as β-hydroxybutyrate) contribute to sterol synthesis [34], which is essential for the growth of myelin membranes [35]. Studies have shown that diabetic patients can significantly increase HDL cholesterol (HDLc) and lower blood pressure through a 90-day KD, while LDL cholesterol shows no significant difference [36]. However, long-term KD consumption increases the risk of type 2 diabetes and metabolic syndrome. This study explored the relevant mechanism of short-term KD treatment in SCI rats [37]. Additionally, studies have found that HDLc showed small increases after ketogenic phases, but there was no significant change over 12 months [38].

This study also found that myelin areas were significantly larger in SCI rats after being fed a KD than in SCI rats in the SD group. A recent study by Stumpf found that a KD can improve axon defects and promote myelination in Pelizaeus-Merzbacher disease. A high-fat/low-carbohydrate KD can restore the integrity of oligodendrocytes and increase CNS myelin. Lipids (such as ketone bodies) easily enter the CNS without destroying the blood-brain barrier or blood-spinal cord barrier [39]. Ketone bodies produced by a SD are not able to enter the CNS to enhance the myelin membrane. These conclusions indicate that a KD mediates steroid metabolism reprogramming after SCI, facilitates myelin membrane synthesis, promotes myelin sheath regeneration, plays a unique role in neuroprotection, and does not destroy the blood spinal cord barrier function. It is well known that the blood spinal cord barrier is an important barrier for the spinal cord to maintain neuroimmune balance.

This study combined 4 groups of rat genes into the same gene network through WGCNA to analyse the correlation between gene modules and phenotype. Through module identification and analysis as well as GO function and KEGG pathway analyses, we showed that rats fed a KD displayed significantly reduced immune-related pathways, including immune diseases and infectious diseases. In addition, examining the data from the SCI_KD and SCI_SD groups and existing MSigDB analysed by GSEA, we concluded that SCI_KD is significantly negatively correlated with inflammatory cytokines and their receptors. These results indicate that KD treatment can improve the body's immunity and reduce infection and inflammation.

In SCI secondary injury, inflammation is an important and main pathophysiological process. After SCI, ischaemia-reperfusion injury, endothelial cell injury and homeostasis disorders jointly initiate the inflammatory cascade reaction, and spinal cord innate immune cells (microglia and astrocytes) [40] and infiltrating white blood cells (neutrophils and macrophages) are activated [40–41]. The activated inflammatory cells release a large number of inflammatory factors to further expand the damage and increase the time and space of the damage response. Our research has shown that KD reduces or inhibits neutrophils in the plasma of SCI rats and inhibits the classic NF-κB pro-inflammatory signalling pathway at the injury site, which corresponds to the results of this study [17]. Steroid synthesis is also closely related to SCI neuroinflammation, and steroid synthesis hormones [42], oestrogen [43–44], saponin [45], tauroursodeoxycholic acid [46] and other steroid components in SCI all have anti-inflammatory properties. Figure 6A–6B show the KEGG signalling pathway at the intersection of the immune microenvironment of a SD and a KD, respectively. The SD mainly activates innate immune-related pathways, such as the Toll-like receptor signalling pathway and NOD-like receptor signalling pathway. This study cannot directly prove a correlation between KD-mediated reprogramming of steroid metabolism and neuroimmunity, which is the limitation of the study. The significantly expressed genes in the steroid synthesis pathway need to be further examined in future studies to determine if they are related to SCI efficacy.

CONCLUSIONS

This study is the first to demonstrate that the KD significantly promotes the reprogramming of steroid metabolism in the treatment of SCI at the transcriptional level. These changes are beneficial for myelin sheath growth and promote nerve function. Moreover, a comprehensive analysis of the KD through WGCNA indicates the improvement of the SCI immune microenvironment and reduction in inflammation. Therefore, we believe that the KD may improve the immune microenvironment and myelin growth in rats with SCI through the reprogramming of steroid metabolism.

METHODS

Animals and diets

All animal experiments conformed to the Guide for the Care and Use of Laboratory Animals (NIH Publications No. 8023, revised 1978). All procedures and euthanasia performed in this study were approved by the Ethics Committee for Animal Experiments of the Department of Laboratory Animal Science, Peking University Health Science Center (No. LA201456, 24 February 2014).

We randomly divided 32 8-week-old male Sprague-Dawley rats (300–360 g) into the following four groups (n = 8 in each group): the control group was undamaged and divided into the SD group (Sham_SD) and the KD group (Sham_KD), while the SCI rats received either the SD (SCI_SD group) or KD (SCI_KD group); 20 rats were used for RNA-seq, and 12 rats were used for histopathological examination of fixed specimens. All rats were reared at 21°C with a light/dark cycle of 12/12 hours, and food and water were provided freely. Rats in the SCI_KD group were fed a KD (70 g/kg body weight/day), and the ratio of fat to carbohydrate and protein was 4:1 (fat: 50.5 g/100 g KD; carbohydrate: 23.6 g/100; four hours after SCI, protein content: 5.5 g/100 g KD; dietary fibre: 16.1 g/100 g KD (Shenzhen Zeneca Inc., Shenzhen, China)). The rats in the Sham_SD group and SCI _SD group were fed normal carbohydrates. All groups had free-access water supply.

C7 spinal cord semi-contusion

A C7 hemi-contusion was performed in the two SCI groups as described previously for a different site of contusion [20]. Briefly, rats were anaesthetized with sodium pentobarbital after a unilateral (left or right side, chosen randomly) C7 laminectomy, and the C6-T1 vertebrae were rigidly fixed in a frame tilted at a 25.0° angle. We then used an Infinite Horizon impactor to deliver a set contusion force of 150 kdyne [21]. The C7 hemi-contusion is hereafter described as 'SCI.' Rats were fed for four weeks according to the above grouping and diet plan, and spinal cord tissue was sampled after four weeks.

EC myelin staining

Spinal cord tissue was placed in a fully automatic tissue dehydrator for an overnight dehydration programme (xylene, alcohol isocratic dehydration), embedded in paraffin, and cut it into 5-µm continuous sections with a microtome after cooling overnight at 40°C. The tissues were soaked in xylene I and II for 30 minutes each, after which they were soaked in 100%, 100%, 95%, 95%, and 80% alcohol for 5 minutes each and then rinsed twice with double-distilled water. The tissues were then stained with eriochrome cyanine (EC) for 15–20 minutes before undergoing ferric chloride (5.6%) differentiation for a specific time under a microscope. We made sure not to over-differentiate, as the staining would be too light. Afterwards, the samples were dehydrated and mounted with neutral gum.

RNA isolation, RNA-seq library construction and sequencing

We randomly divided 20 Sprague-Dawley rats into 4 groups: SCI_KD; SCI_SD; Sham_KD; and Sham_SD. Total RNA was extracted from a 1.6-cm spinal cord segment at the centre of the impact site with the TRIzol reagent (Invitrogen, Thermo Fisher Scientific Inc., MA, USA) and subjected to RNA-seq analysis to assess gene expression ($n = 5$). Genomic DNA was removed using DNase I. Agarose gels (1%) were used to monitor RNA degradation and contamination. A NanoPhotometer® spectrophotometer (IMPLEN, CA, USA) was used to check RNA purity. A Qubit® RNA Assay Kit was used to measure the RNA concentration on a Qubit® 2.0 Fluorometer (Life Technologies, CA, USA). An RNA Nano 6000 Assay Kit was used to assess the RNA integrity on a Bioanalyser 2100 system (Agilent Technologies, CA, USA). RNA sequencing of 5 biological replicate samples was performed for each group, and 5 samples were degraded and eliminated. Therefore, 15 RNA-seq cDNA libraries were established.

1) We utilized two methods to treat the total RNA. Oligo(dT) magnetic beads were used to select mRNAs with polyA tails. rRNAs were hybridized with DNA probes and then digested to generate a DNA/RNA hybrid strand, followed by DNase I digestion to remove DNA probes. The target RNAs were then obtained by purification. 2) The target RNA was fragmented and then reverse transcribed into double-stranded cDNA (dscDNA) with N6 random primers. 3) The dscDNA was end-repaired with phosphates at the 5′ end and sticky ′A′s at the 3' end, after which the sequence was ligated to an adaptor with sticky 'T's at the 3' end of the dscDNA. 4) Two specific primers were used to amplify the ligation product. 5) The PCR products were denatured with heat, and the single strand DNA was cyclized with a splint oligo and DNA ligase. 6) Finally, the prepared library was sequenced with the Illumina HiSeq xten (2×150-bp read length, Illumina, San Diego, CA, USA). The sequencing programmes were performed by BGI Company (China, Shenzhen).

Quality control and expression level

The raw paired-end reads were trimmed and subjected to quality control by SeqPrep (https://github.com/jstjohn/SeqPrep) and Sickle (https://github.com/najoshi/sickle) with default parameters. The paired-end clean reads were aligned to the Rattus_norvegicus reference genome (Rnor_6.0) using the default parameters in TopHat (http://tophat.cbcb.umd.edu/, version 2.1.1) [47]. The reference genome and gene model annotation files

were directly downloaded from genome website (http://www.ensembl.org/Rattus_norvegicus/Info/Index). RSEM (http://deweylab.biostat.wisc.Edu/rsem/) [48] was used to quantify the gene abundances. To identify DEGs between two different samples, the expression levels of each transcript were calculated based on the number of transcript reads per million reads (TPM). The reads were then normalized using DESeq2 version 1.24.0 (http://bioconductor.org/packages/stats/bioc/DESeq2/) [49], and the statistical significance of the DEGs was assessed. The following default parameters and criteria were used here: Benjamini & Hochberg (BH) p-adjust < 0.05 and |log2FC|≥1 after multiple comparisons. In the initial data exploration, we performed principal component analysis (PCA) to directly calculate the coefficient of variation between the groups in R 'prcomp'.

Gene function annotation analysis

The genes and transcripts are aligned to six databases (NR, Swiss-Prot, Pfam, EggNOG, GO, and KEGG) to obtain comprehensive annotation information. DIAMOND software (https://github.com/bbuchfink/diamond) [50] was used to sequence the genes and transcripts with the NR (ftp://ftp.ncbi.nlm.nih.gov/blast/db/), Swiss-Prot (ftp://ftp.uniprot.org/pub/databases), and EggNOG (http://eggnogdb.embl.de/#/app/home) databases [51]. Sequence alignment was performed with the BLAST2GO and GO database, followed by alignment with the Pfam database using HMMER software [52]. GO (http://www.geneontology.org/) is a database established by the Gene Ontology Federation. Its purpose is to standardize the biological terminology of genes and gene products in different databases and to determine gene and protein functions. Using the GO database, the genes in the selected gene set can be classified according to the biological process (BP) they participate in, the cell component (CC), and the molecular function (MF) they achieve. The results of KEGG Orthology (Kyoto Encyclopaedia of Genes and Genomes, http://www.genome.jp/kegg/) were obtained using KOBAS2.1. KEGG is a knowledge base that systematically analyses gene functions and links genomic information and functional information. Using the KEGG database, the genes in the gene set can be classified according to the pathways involved or the functions they perform [53].

KEGG pathway enrichment analysis

The KEGG PATHWAY enrichment analysis was performed on the gene set using an R script in KOBAS (http://kobas.cbi.pku.edu.cn/home.do) [53]. The BH method was used to calculate the corrected p value. The threshold of the corrected p value (corrected P-value)

was 0.05. The KEGG pathway that met the conditions showed that the pathway was significantly enriched for the gene set.

iPath metabolic pathway analysis

iPath3.0 (http://pathways.embl.de) was used to visually analyse the metabolic pathways and facilitate observation of the metabolic pathway information of DEGs in the entire biological system. Nodes represent various biochemical molecules, and lines represent biochemical reactions. The overall metabolism of the biological system includes 146 metabolism-related KEGG pathways, 22 regulatory-related KEGG pathways, and 58 KEGG pathways involved in the biosynthesis of secondary metabolites. The nodes in the figure represent different compounds, and the boundaries represent different enzymatic reactions. iPath3.0 can outline the biosynthesis and important regulatory pathways of secondary metabolites and easily identify complex metabolic pathways [54].

Gene set enrichment analysis (GSEA)

GSEA is performed on a predefined set of genes, usually from functional annotations or the results of previous experiments (included in MSigDB, version 6.2, http://software.broadinstitute.org/gsea/downloads.jsp), and organizes the genes according to two sample types. The GSEA sorts the degree of differential expression and then checks whether the gene set clusters at the top or bottom of the ranking list. The first round of enrichment is based on C2, which includes curated gene sets (from online pathway databases, publications in PubMed, and knowledge of domain experts). The second enrichment is based on the results of KEGG functional annotation in this study. For the analysis results, we generally considered that gene sets with the following characteristics were meaningful: $|NES|>1$, NOM p-val<0.05, and FDR q-val<0.25.

Protein-protein interaction (PPI) analysis

We used an online search tool (STRING database, version 10.5; http://string-db.org/) to search for interacting genes to construct a protein-protein interaction (PPI) network based on the extensive functions of the genome-wide data [55].

Weighted gene co-expression network analysis (WGCNA)

A co-expression network was constructed using the WGCNA (version 1.47) package in R [21]. WGCNA is an undirected, weighted network. "Unweighted network" means that the correlation between genes can

only be 0 or 1. 0 means that the two genes are not related, while 1 means they are related. A "weighted network" means not only that genes are related or not but also that their correlation value is recorded. The value is the weight (correlation) of the connection between genes. The soft threshold (β power) in the co-expression network is the expression of each gene at a specific time or space and is regarded as a node. To obtain the correlation between genes, it is necessary to calculate the correlation coefficient (Pearson coefficient) any two genes; this allows us to know whether the expression profiles of two genes are similar. In this study, the β power = 6.

1) The module refers to the grouping of genes with similar expression patterns. Genes of a specific type below to a module.

2) An eigengene is defined as the first principal component of a given module. It is the most representative expression pattern of the module. It is an indicator that approximately represents the expression status of all genes in a module but is not a real gene.

3) A hub module refers to a module that is highly related to phenotypic data or closely related to research.

4) Gene significance (GS), or a measure of gene importance, is the correlation between gene expression patterns and the characteristics of a sample. Generally, the larger the correlation value, the more important the gene, which can be evaluated as the log conversion of the p-value. The correlation index between a gene and a specific pathway can also be the correlation between a gene and a specific phenotypic feature.

5) Module membership (MM), also known as the eigengene-based connectivity (kME), is the correlation between the expression pattern of a gene and a characteristic gene in the module. The larger the value, the greater the possibility that the gene belongs to the module.

Genes with the highest MM and the highest GS are genes with high significance (hub genes). All these analyses were performed using commands implemented in the WGCNA software package with the following parameters: minModuleSize = 30, minKMEtoStay = 0.3, and mergeCutHeight = 0.2.

Modular gene expression correlation analysis

After a gene of interest is obtained based on the correlation of gene expression, the correlation coefficient between genes is determined using the Spearman correlation algorithm. The correlation

coefficient threshold is 0.5, the significance level is the *p* value after BH correction (corrected *p*-value) ≤0.05, and these values were drawn into a visual network diagram. In the figure, the nodes represent genes, and the connections between nodes represent the correlation between gene expression. The larger the node is, the greater the expression correlation between the genes.

Multi-gene set KEGG pathway enrichment analysis

After performing KEGG analysis on the different gene sets, we utilized the intersection of the selected gene sets for the display and adjusted the significance level to the corrected *p*-value ≤0.5 as the threshold to display the top 20 pathways.

Statistical analysis

The data are expressed as the mean ± standard deviation. The statistical analysis was performed with GraphPad Prism 7.0 (GraphPad Software Inc., San Diego, CA). Student's *t*-test was used for comparisons between two groups. A *p* value < 0.05 was considered statistically significant. $^*p < 0.05$, $^{**}p < 0.01$, $^{***}p < 0.001$, and $^{****}p < 0.0001$.

Availability of data and materials

RNA-seq raw data have been deposited in the NCBI Sequence Read Archive (SRA, https://submit.ncbi.nlm.nih.gov/subs/sra/SUB7836712/overview). Accession IDs for *Rattus norvegicus* BioProject = PRJNA648739; BioSample = SAMN15646629 – SAMN15646643 (15 objects); SRA = SRR12327118 – SRR12327132 (15 objects).

Abbreviations

SCI: spinal cord Injury; RNA-seq: RNA sequencing; CNS: central nervous system; KD: ketogenic diet; WGCNA: weighted gene co-expression network analysis; PPI: protein-protein interaction; GSEA: gene set enrichment analysis; DEGs: differentially expressed genes; GO: Gene ontology; KEGG: Kyoto Encyclopedia of Genes and Genomes; GS: gene significance; MM: module membership.

AUTHOR CONTRIBUTIONS

MWZ, HZ and YL conceived and designed the study, MWZ coordinated the project and partly wrote the manuscript. HZ and YL performed animals management and bio-samples collection. HZ, YL, MJH, YYY, HYX, XXL designed analyses, performed bioinformatic analyses and partly wrote the manuscript. MWZ supervised and performed bioinformatic analyses. HZ and YL wrote and revised the article. All these authors read and approved the final manuscript.

CONFLICTS OF INTEREST

The authors declare no conflicts of interest related to this study.

REFERENCES

1. Fakhoury M. Spinal cord injury: overview of experimental approaches used to restore locomotor activity. Rev Neurosci. 2015; 26:397–405.
   https://doi.org/10.1515/revneuro-2015-0001
   PMID:25870961

2. Bravo-Esteban E, Taylor J, Aleixandre M, Simón-Martínez C, Torricelli D, Pons JL, Avila-Martín G, Galán-Arriero I, Gómez-Soriano J. Longitudinal estimation of intramuscular Tibialis Anterior coherence during subacute spinal cord injury: relationship with neurophysiological, functional and clinical outcome measures. J Neuroeng Rehabil. 2017; 14:58.
   https://doi.org/10.1186/s12984-017-0271-9
   PMID:28619087

3. Fitch MT, Doller C, Combs CK, Landreth GE, Silver J. Cellular and molecular mechanisms of glial scarring and progressive cavitation: *in vivo* and *in vitro* analysis of inflammation-induced secondary injury after CNS trauma. J Neurosci. 1999; 19:8182–98.
   https://doi.org/10.1523/JNEUROSCI.19-19-08182.1999
   PMID:10493720

4. Kjell J, Olson L. Rat models of spinal cord injury: from

pathology to potential therapies. Dis Model Mech. 2016; 9:1125–37.
https://doi.org/10.1242/dmm.025833
PMID:27736748

5. Shultz RB, Zhong Y. Minocycline targets multiple secondary injury mechanisms in traumatic spinal cord injury. Neural Regen Res. 2017; 12:702–13.
https://doi.org/10.4103/1673-5374.206633
PMID:28616020

6. Orr MB, Gensel JC. Spinal Cord Injury Scarring and Inflammation: Therapies Targeting Glial and Inflammatory Responses. Neurotherapeutics. 2018; 15:541–53.
https://doi.org/10.1007/s13311-018-0631-6
PMID:29717413

7. Yılmaz T, Kaptanoğlu E. Current and future medical therapeutic strategies for the functional repair of spinal cord injury. World J Orthop. 2015; 6:42–55.
https://doi.org/10.5312/wjo.v6.i1.42
PMID:25621210

8. Keene DL. A systematic review of the use of the ketogenic diet in childhood epilepsy. Pediatr Neurol. 2006; 35:1–5.
https://doi.org/10.1016/j.pediatrneurol.2006.01.005
PMID:16814077

9. Stafstrom CE, Rho JM. The ketogenic diet as a treatment paradigm for diverse neurological disorders. Front Pharmacol. 2012; 3:59.
https://doi.org/10.3389/fphar.2012.00059
PMID:22509165

10. Winesett SP, Bessone SK, Kossoff EH. The ketogenic diet in pharmacoresistant childhood epilepsy. Expert Rev Neurother. 2015; 15:621–28.
https://doi.org/10.1586/14737175.2015.1044982
PMID:25994046

11. Paoli A, Bianco A, Damiani E, Bosco G. Ketogenic diet in neuromuscular and neurodegenerative diseases. Biomed Res Int. 2014; 2014:474296.
https://doi.org/10.1155/2014/474296
PMID:25101284

12. Shaafi S, Sharifi-Bonab M, Ghaemian N, Mokhtarkhani M, Akbari H. Early Motor-Behavioral Outcome of Ischemic Stroke with Ketogenic Diet Preconditioning: Interventional Animal Study. J Stroke Cerebrovasc Dis. 2019; 28:1032–39.
https://doi.org/10.1016/j.jstrokecerebrovasdis.2018.12.024
PMID:30658953

13. McDougall A, Bayley M, Munce SE. The ketogenic diet as a treatment for traumatic brain injury: a scoping review. Brain Inj. 2018; 32:416–22.
https://doi.org/10.1080/02699052.2018.1429025
PMID:29359959

14. Streijger F, Plunet WT, Lee JH, Liu J, Lam CK, Park S, Hilton BJ, Fransen BL, Matheson KA, Assinck P, Kwon BK, Tetzlaff W. Ketogenic diet improves forelimb motor function after spinal cord injury in rodents. PLoS One. 2013; 8:e78765.
https://doi.org/10.1371/journal.pone.0078765
PMID:24223849

15. Yarar-Fisher C, Kulkarni A, Li J, Farley P, Renfro C, Aslam H, Bosarge P, Wilson L, Barnes S. Evaluation of a ketogenic diet for improvement of neurological recovery in individuals with acute spinal cord injury: a pilot, randomized safety and feasibility trial. Spinal Cord Ser Cases. 2018; 4:88.
https://doi.org/10.1038/s41394-018-0121-4
PMID:30275980

16. Liu Q, Wang X, Huang Z, Liu J, Ding J, Xu X, Kong G, Wu X, Yang Z, Zhu Q. Ketogenic diet delays spinal fusion and decreases bone mass in posterolateral lumbar spinal fusion: an *in vivo* rat model. Acta Neurochir (Wien). 2018; 160:1909–16.
https://doi.org/10.1007/s00701-018-3616-7
PMID:29982887

17. Lu Y, Yang YY, Zhou MW, Liu N, Xing HY, Liu XX, Li F. Ketogenic diet attenuates oxidative stress and inflammation after spinal cord injury by activating Nrf2 and suppressing the NF-κB signaling pathways. Neurosci Lett. 2018; 683:13–18.
https://doi.org/10.1016/j.neulet.2018.06.016
PMID:29894768

18. Wang X, Wu X, Liu Q, Kong G, Zhou J, Jiang J, Wu X, Huang Z, Su W, Zhu Q. Ketogenic Metabolism Inhibits Histone Deacetylase (HDAC) and Reduces Oxidative Stress After Spinal Cord Injury in Rats. Neuroscience. 2017; 366:36–43.
https://doi.org/10.1016/j.neuroscience.2017.09.056
PMID:29024787

19. Kong G, Huang Z, Ji W, Wang X, Liu J, Wu X, Huang Z, Li R, Zhu Q. The Ketone Metabolite β-Hydroxybutyrate Attenuates Oxidative Stress in Spinal Cord Injury by Suppression of Class I Histone Deacetylases. J Neurotrauma. 2017; 34:2645–55.
https://doi.org/10.1089/neu.2017.5192
PMID:28683591

20. Yokoi A, Yoshioka Y, Yamamoto Y, Ishikawa M, Ikeda SI, Kato T, Kiyono T, Takeshita F, Kajiyama H, Kikkawa F, Ochiya T. Malignant extracellular vesicles carrying MMP1 mRNA facilitate peritoneal dissemination in ovarian cancer. Nat Commun. 2017; 8:14470.
https://doi.org/10.1038/ncomms14470
PMID:28262727

21. Huynh NPT, Zhang B, Guilak F. High-depth

transcriptomic profiling reveals the temporal gene signature of human mesenchymal stem cells during chondrogenesis. FASEB J. 2019; 33:358–72. https://doi.org/10.1096/fj.201800534R PMID:29985644

22. Martin K, Jackson CF, Levy RG, Cooper PN. Ketogenic diet and other dietary treatments for epilepsy. Cochrane Database Syst Rev. 2016; 2:CD001903. https://doi.org/10.1002/14651858.CD001903.pub3 PMID:26859528

23. Li RJ, Liu Y, Liu HQ, Li J. Ketogenic diets and protective mechanisms in epilepsy, metabolic disorders, cancer, neuronal loss, and muscle and nerve degeneration. J Food Biochem. 2020; 44:e13140. https://doi.org/10.1111/jfbc.13140 PMID:31943235

24. Veyrat-Durebex C, Reynier P, Procaccio V, Hergesheimer R, Corcia P, Andres CR, Blasco H. How Can a Ketogenic Diet Improve Motor Function? Front Mol Neurosci. 2018; 11:15. https://doi.org/10.3389/fnmol.2018.00015 PMID:29434537

25. Demirel A, Li J, Morrow C, Barnes S, Jansen J, Gower B, Kirksey K, Redden D, Yarar-Fisher C. Evaluation of a ketogenic diet for improvement of neurological recovery in individuals with acute spinal cord injury: study protocol for a randomized controlled trial. Trials. 2020; 21:372. https://doi.org/10.1186/s13063-020-04273-7 PMID:32366293

26. Lee PR, Kossoff EH. Dietary treatments for epilepsy: management guidelines for the general practitioner. Epilepsy Behav. 2011; 21:115–21. https://doi.org/10.1016/j.yebeh.2011.03.008 PMID:21514240

27. Broom GM, Shaw IC, Rucklidge JJ. The ketogenic diet as a potential treatment and prevention strategy for Alzheimer's disease. Nutrition. 2019; 60:118–21. https://doi.org/10.1016/j.nut.2018.10.003 PMID:30554068

28. Webster CC, Murphy TE, Larmuth KM, Noakes TD, Smith JA. Diet, Diabetes Status, and Personal Experiences of Individuals with Type 2 diabetes Who Self-Selected and Followed a Low Carbohydrate High Fat diet. Diabetes Metab Syndr Obes. 2019; 12:2567–82. https://doi.org/10.2147/DMSO.S227090 PMID:31827331

29. Burke LM. Ketogenic low-CHO, high-fat diet: the future of elite endurance sport? J Physiol. 2021; 599:819–43. https://doi.org/10.1113/JP278928 PMID:32358802

30. Cerqueira NM, Oliveira EF, Gesto DS, Santos-Martins D, Moreira C, Moorthy HN, Ramos MJ, Fernandes PA. Cholesterol Biosynthesis: A Mechanistic Overview. Biochemistry. 2016; 55:5483–506. https://doi.org/10.1021/acs.biochem.6b00342 PMID:27604037

31. Straub RH, Cutolo M. Glucocorticoids and chronic inflammation. Rheumatology (Oxford). 2016 (Suppl 2); 55:ii6–14. https://doi.org/10.1093/rheumatology/kew348 PMID:27856655

32. Ur Rahman S, Ismail M, Khurram M, Ullah I, Rabbi F, Iriti M. Bioactive Steroids and Saponins of the Genus Trillium. Molecules. 2017; 22:2156. https://doi.org/10.3390/molecules22122156 PMID:29206216

33. Koper JW, Lopes-Cardozo M, Van Golde LM. Preferential utilization of ketone bodies for the synthesis of myelin cholesterol *in vivo*. Biochim Biophys Acta. 1981; 666:411–17. https://doi.org/10.1016/0005-2760(81)90300-3 PMID:7326251

34. Saher G, Brügger B, Lappe-Siefke C, Möbius W, Tozawa R, Wehr MC, Wieland F, Ishibashi S, Nave KA. High cholesterol level is essential for myelin membrane growth. Nat Neurosci. 2005; 8:468–75. https://doi.org/10.1038/nn1426 PMID:15793579

35. Walton CM, Perry K, Hart RH, Berry SL, Bikman BT. Improvement in Glycemic and Lipid Profiles in Type 2 Diabetics with a 90-Day Ketogenic Diet. J Diabetes Res. 2019; 2019:8681959. https://doi.org/10.1155/2019/8681959 PMID:31485454

36. Ellenbroek JH, van Dijck L, Töns HA, Rabelink TJ, Carlotti F, Ballieux BE, de Koning EJ. Long-term ketogenic diet causes glucose intolerance and reduced β- and α-cell mass but no weight loss in mice. Am J Physiol Endocrinol Metab. 2014; 306:E552–58. https://doi.org/10.1152/ajpendo.00453.2013 PMID:24398402

37. Paoli A, Bianco A, Grimaldi KA, Lodi A, Bosco G. Long term successful weight loss with a combination biphasic ketogenic Mediterranean diet and Mediterranean diet maintenance protocol. Nutrients. 2013; 5:5205–17. https://doi.org/10.3390/nu5125205 PMID:24352095

38. Stumpf SK, Berghoff SA, Trevisiol A, Spieth L, Düking T, Schneider LV, Schlaphoff L, Dreha-Kulaczewski S, Bley A, Burfeind D, Kusch K, Mitkovski M, Ruhwedel T, et al. Correction to: ketogenic diet ameliorates axonal defects

and promotes myelination in Pelizaeus-Merzbacher disease. Acta Neuropathol. 2019; 138:673–74.
https://doi.org/10.1007/s00401-019-02064-2
PMID:31482207

39. Zeng H, Liu N, Yang YY, Xing HY, Liu XX, Li F, La GY, Huang MJ, Zhou MW. Lentivirus-mediated downregulation of α-synuclein reduces neuroinflammation and promotes functional recovery in rats with spinal cord injury. J Neuroinflammation. 2019; 16:283.
https://doi.org/10.1186/s12974-019-1658-2
PMID:31888724

40. Milich LM, Ryan CB, Lee JK. Correction to: the origin, fate, and contribution of macrophages to spinal cord injury pathology. Acta Neuropathol. 2019; 137:799–800.
https://doi.org/10.1007/s00401-019-02016-w
PMID:31011858

41. Li Y, Gu R, Zhu Q, Liu J. Changes of Spinal Edema and Expression of Aquaporin 4 in Methylprednisolone-treated Rats with Spinal Cord Injury. Ann Clin Lab Sci. 2018; 48:453–59.
PMID:30143486

42. Lee JY, Choi HY, Ju BG, Yune TY. Estrogen alleviates neuropathic pain induced after spinal cord injury by inhibiting microglia and astrocyte activation. Biochim Biophys Acta Mol Basis Dis. 2018; 1864:2472–80.
https://doi.org/10.1016/j.bbadis.2018.04.006
PMID:29653184

43. Zendedel A, Mönnink F, Hassanzadeh G, Zaminy A, Ansar MM, Habib P, Slowik A, Kipp M, Beyer C. Estrogen Attenuates Local Inflammasome Expression and Activation after Spinal Cord Injury. Mol Neurobiol. 2018; 55:1364–75.
https://doi.org/10.1007/s12035-017-0400-2
PMID:28127698

44. Chen XB, Wang ZL, Yang QY, Zhao FY, Qin XL, Tang XE, Du JL, Chen ZH, Zhang K, Huang FJ. Diosgenin Glucoside Protects against Spinal Cord Injury by Regulating Autophagy and Alleviating Apoptosis. Int J Mol Sci. 2018; 19:2274.
https://doi.org/10.3390/ijms19082274
PMID:30072674

45. Zhang Z, Chen J, Chen F, Yu D, Li R, Lv C, Wang H, Li H, Li J, Cai Y. Tauroursodeoxycholic acid alleviates secondary injury in the spinal cord via up-regulation of CIBZ gene. Cell Stress Chaperones. 2018; 23:551–60.
https://doi.org/10.1007/s12192-017-0862-1
PMID:29151236

46. Trapnell C, Pachter L, Salzberg SL. TopHat: discovering splice junctions with RNA-Seq. Bioinformatics. 2009; 25:1105–11.
https://doi.org/10.1093/bioinformatics/btp120
PMID:19289445

47. Li B, Dewey CN. RSEM: accurate transcript quantification from RNA-Seq data with or without a reference genome. BMC Bioinformatics. 2011; 12:323.
https://doi.org/10.1186/1471-2105-12-323
PMID:21816040

48. Love MI, Huber W, Anders S. Moderated estimation of fold change and dispersion for RNA-seq data with DESeq2. Genome Biol. 2014; 15:550.
https://doi.org/10.1186/s13059-014-0550-8
PMID:25516281

49. Buchfink B, Xie C, Huson DH. Fast and sensitive protein alignment using DIAMOND. Nat Methods. 2015; 12:59–60.
https://doi.org/10.1038/nmeth.3176
PMID:25402007

50. Powell S, Forslund K, Szklarczyk D, Trachana K, Roth A, Huerta-Cepas J, Gabaldón T, Rattei T, Creevey C, Kuhn M, Jensen LJ, von Mering C, Bork P. eggNOG v4.0: nested orthology inference across 3686 organisms. Nucleic Acids Res. 2014; 42:D231–39.
https://doi.org/10.1093/nar/gkt1253
PMID:24297252

51. Finn RD, Clements J, Eddy SR. HMMER web server: interactive sequence similarity searching. Nucleic Acids Res. 2011 (Suppl 2); 39:W29–37.
https://doi.org/10.1093/nar/gkr367
PMID:21593126

52. Xie C, Mao X, Huang J, Ding Y, Wu J, Dong S, Kong L, Gao G, Li CY, Wei L. KOBAS 2.0: a web server for annotation and identification of enriched pathways and diseases. Nucleic Acids Res. 2011 (Suppl 2); 39:W316–22.
https://doi.org/10.1093/nar/gkr483
PMID:21715386

53. Teng L, Fan X, Xu D, Zhang X, Mock T, Ye N. Identification of Genes under Positive Selection Reveals Differences in Evolutionary Adaptation between Brown-Algal Species. Front Plant Sci. 2017; 8:1429.
https://doi.org/10.3389/fpls.2017.01429
PMID:28861104

54. Szklarczyk D, Morris JH, Cook H, Kuhn M, Wyder S, Simonovic M, Santos A, Doncheva NT, Roth A, Bork P, Jensen LJ, von Mering C. The STRING database in 2017: quality-controlled protein-protein association networks, made broadly accessible. Nucleic Acids Res. 2017; 45:D362–68.
https://doi.org/10.1093/nar/gkw937
PMID:27924014

55. Golonka RM, Xiao X, Abokor AA, Joe B, Vijay-Kumar M. Altered nutrient status reprograms host inflammation and metabolic health via gut microbiota. J Nutr Biochem. 2020; 80:108360.
https://doi.org/10.1016/j.jnutbio.2020.108360
PMID:32163821

Supplementary Figures
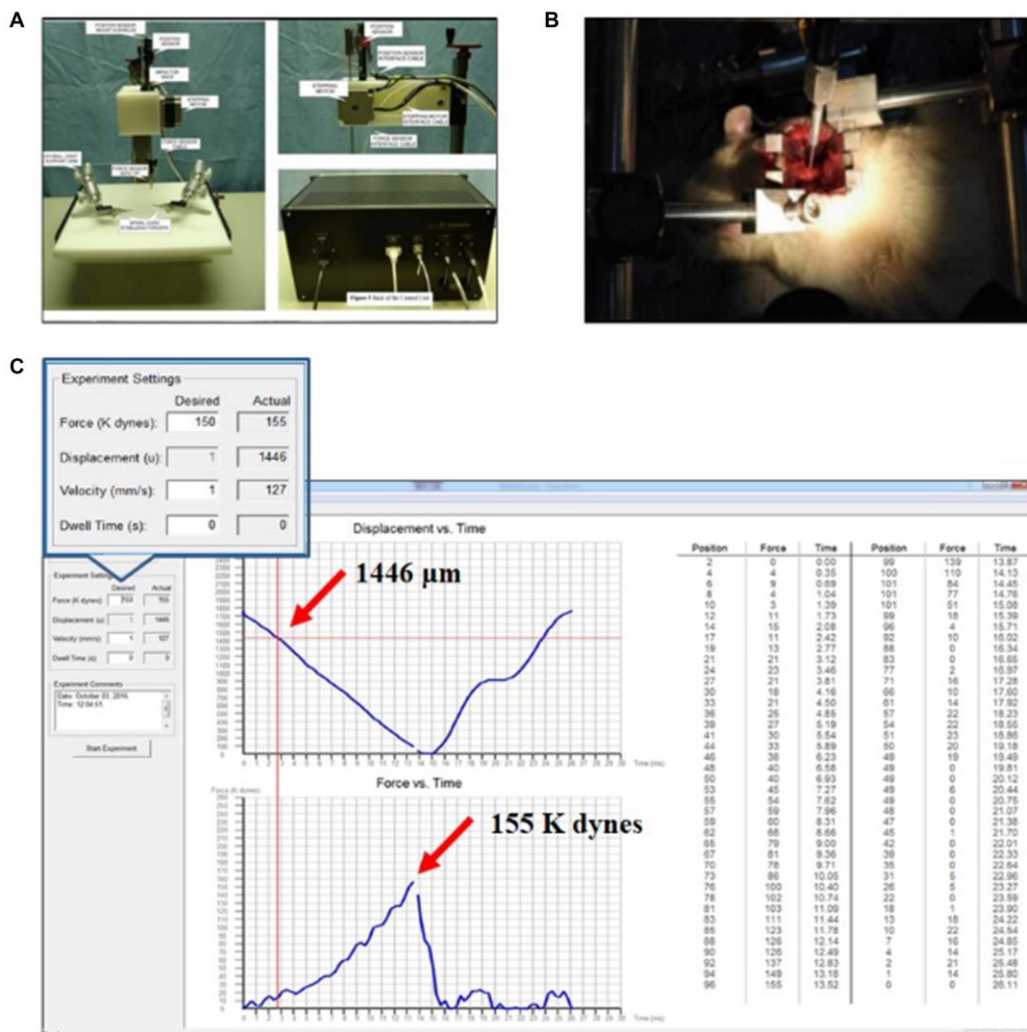
Supplementary Figure 1. Verification of C7 spinal cord hemi-contusion models. (**A**) Representative images of Infinite Horizon impactor. (**B**) Representative images of C6-T1 vertebrae fixed in a frame tilted at a 25.0° angle. (**C**) Representative images of monitoring data after striking by the Infinite Horizon impactor.

Supplementary Figure 2. GSEA showing that SCI_KD and D are significantly negatively correlated with inflammatory cytokines and their receptors, and the NES values are -1.44 (**A**) and -1.46 (**B**), respectively.

Supplementary Figure 3. Visual analysis of enriched steroid metabolism-related genes using iPath3.0.
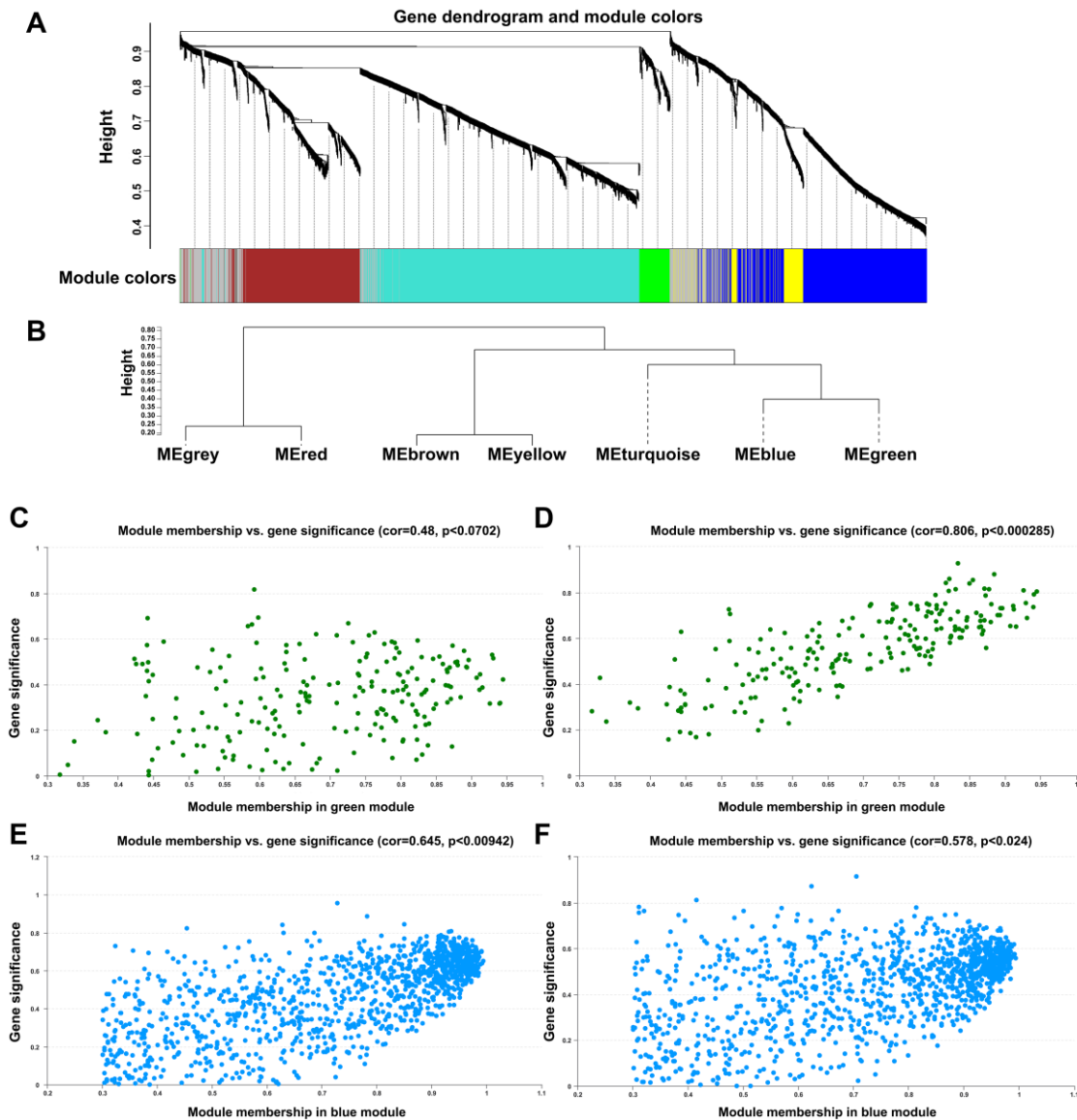
Supplementary Figure 4. Visualization of WGCNA analysis features. (**A**) Module clustering tree diagram display, in which branches represent a module. The closer two modules are branched, the closer the distance between the two modules. (**B**) Gene clustering tree (dendrogram) obtained by hierarchical clustering based on adjacent dissimilarity. (**C**–**D**) MM-GS analysis of the MEgreen module, in which C shows the SCI group, and D shows the Sham group. (**E**–**F**) MM-GS analysis of the MEblue module, in which E shows the SCI group, and F shows the Sham group.
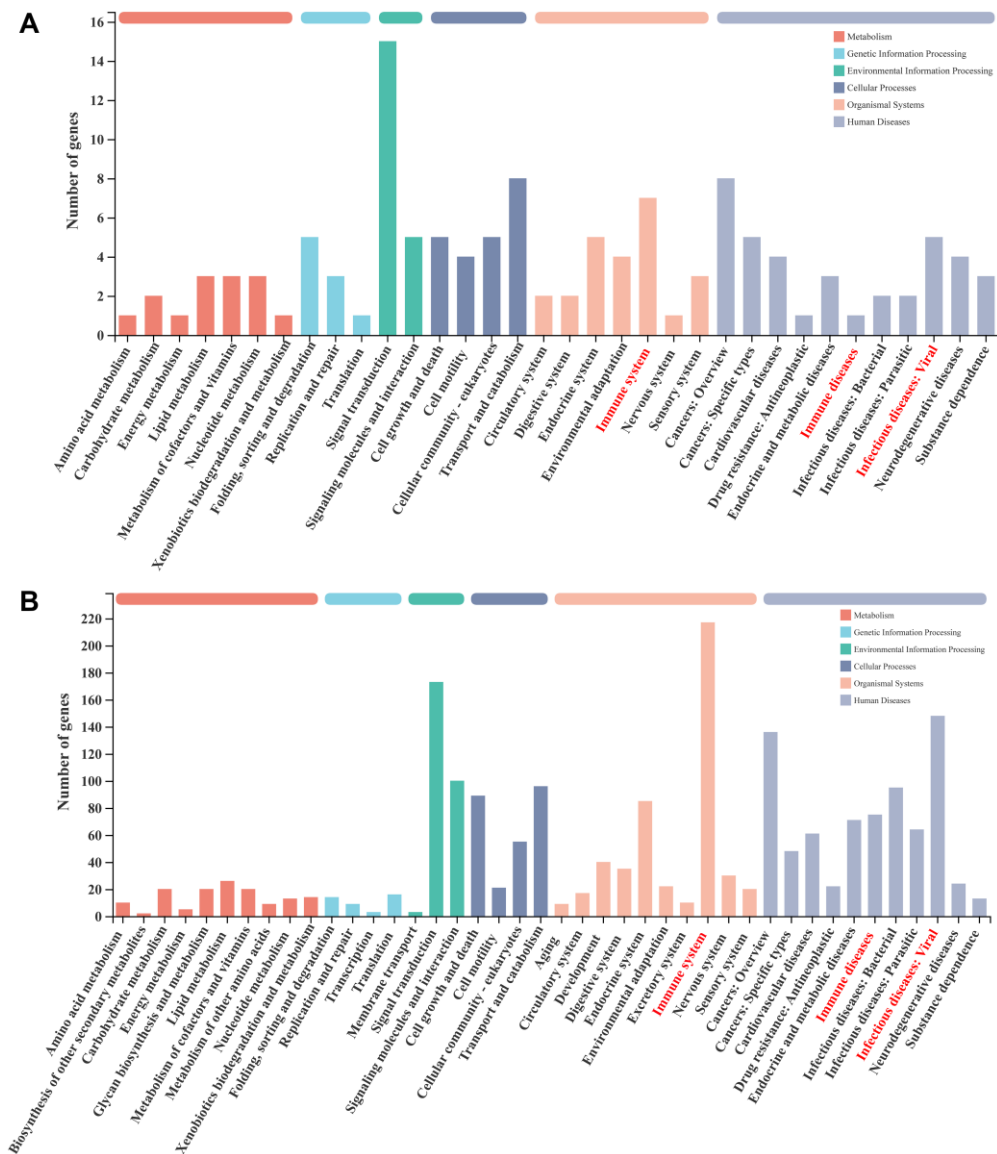
Supplementary Figure 5. Analysis of WGCNA module genes by KEGG pathway annotation. (**A**) The KEGG pathway annotation analysis histogram of the MEgreen module. (**B**) The KEGG pathway annotation analysis histogram of the MEblue module, in which the red font indicates items with significant changes in the green and blue modules.

Supplementary Tables

Supplementary Table 1. Summary of Illumina post-sequencing sequence assembly.

Sample	Clean reads	Clean bases	Error rate (%)	Q20 (%)	Q30 (%)	GC content (%)
SCI_KD1	23065121	1.15E+09	0	100	100	48.6
SCI_KD2	23109839	1.16E+09	0	100	100	48.9
SCI_KD3	23240415	1.16E+09	0	100	100	48.55
SCI_KD4	23094364	1.15E+09	0	100	100	49.56
SCI_KD5	23093374	1.15E+09	0	100	100	49.74
SCI_SD1	23705569	1.19E+09	0	100	100	48.98
SCI_SD2	23294618	1.16E+09	0	100	100	48.71
SCI_SD3	22920879	1.15E+09	0	100	100	48.48
Sham_KD1	23720739	1.19E+09	0	100	100	49.27
Sham_KD2	23702903	1.18E+09	0	100	100	49.77
Sham_KD3	23382678	1.17E+09	0	100	100	49.86
Sham_SD1	23486556	1.17E+09	0	100	100	49.97
Sham_SD2	23150638	1.16E+09	0	100	100	48.86
Sham_SD3	23165313	1.16E+09	0	100	100	48.62
Sham_SD4	21452399	1.07E+09	0	100	100	48.96

Supplementary Table 2. Mapping results between the transcriptome and reference genome.

Sample	Total reads	Total mapped	Multiple mapped	Uniquely mapped
SCI_KD1	23065121	21443709 (92.97%)	2274693 (9.86%)	19169016 (83.11%)
SCI_KD2	23109839	21515285 (93.1%)	2212778 (9.58%)	19302507 (83.53%)
SCI_KD3	23240415	21605446 (92.96%)	2322963 (10.0%)	19282483 (82.97%)
SCI_KD4	23094364	21523546 (93.2%)	2150060 (9.31%)	19373486 (83.89%)
SCI_KD5	23093374	21509560 (93.14%)	2239829 (9.7%)	19269731 (83.44%)
SCI_SD1	23705569	22083424 (93.16%)	2566694 (10.83%)	19516730 (82.33%)
SCI_SD2	23294618	21697617 (93.14%)	2301896 (9.88%)	19395721 (83.26%)
SCI_SD3	22920879	21254877 (92.73%)	2395814 (10.45%)	18859063 (82.28%)
Sham_KD1	23720739	22140211 (93.34%)	2187062 (9.22%)	19953149 (84.12%)
Sham_KD2	23702903	22091787 (93.2%)	2239448 (9.45%)	19852339 (83.75%)
Sham_KD3	23382678	21861517 (93.49%)	2109646 (9.02%)	19751871 (84.47%)
Sham_SD1	23486556	21964601 (93.52%)	2094514 (8.92%)	19870087 (84.6%)
Sham_SD2	23150638	21578282 (93.21%)	2172727 (9.39%)	19405555 (83.82%)
Sham_SD3	23165313	21556978 (93.06%)	2303960 (9.95%)	19253018 (83.11%)
Sham_SD4	21452399	19967854 (93.08%)	2080077 (9.7%)	17887777 (83.38%)

Please browse Full Text version to see the data of Supplementary Tables 3 and 4.

Supplementary Table 3. List of 184 upregulated DEGs expressed between the SCI group and LV_SCI group.

Supplementary Table 4. List of 279 downregulated DEGs expressed between the SCI group and LV_SCI group.

Supplementary Table 5. A statistical table of the number of members (genes/transcripts) contained in each module. The first column is the module (indicated by the colour), and the second column is the number of members belonging to the module.

module	number
blue	1221
brown	873
turquoise	1877
grey	716
yellow	263
green	213